Resolving Power Consumption of Variable Power Electronic Loads Using Nonintrusive Monitoring

Warit Wichakool*, Al-Thaddeus Avestruz*, Robert W. Cox†, Steven B. Leeb*

* LABORATORY OF ELECTROMAGNETIC AND ELECTRONIC SYSTEMS,
MASSACHUSETTS INSTITUTE OF TECHNOLOGY, CAMBRIDGE, MA 02139
EMAIL: waritw@mit.edu

† ELECTRICAL & COMPUTER ENGINEERING,
UNC CHARLOTTE, CHARLOTTE, NC 28223
EMAIL: rcox3@uncc.edu

***Abstract*—This paper demonstrates a new estimator to resolve the average power consumption of a variable-speed drive (VSD) from other constant power loads using a spectral estimation method and a switching function technique for nonintrusive load monitoring (NILM) applications. The estimator uses the rectifier switching function to create adaptive estimating functions for the fundamental power from a finite set of current harmonics generated by the VSD. Experimental results show that the proposed VSD power estimator can significantly improve NILM's ability to resolve the VSD power consumption under small input voltage variation.**

***Index Terms*—nonintrusive load monitoring, rectifier, spectral estimation, switching function, variable-speed drive (VSD).**

I. Introduction

A nonintrusive load monitoring (NILM) system has been developed to detect and track operating conditions and power consumptions of multiple loads from a central location using line current harmonic signatures or spectral envelopes [1]–[5]. The ability to identify and extract load usage information can be useful for scheduling load operation, for optimizing energy consumption, and for detecting various faults. For a constant power load, the identification is accomplished by matching the behavior of spectral envelopes during a transient event and a steady-state operation [1], [4]. On the other hand, a variable power electronic load such as a variable-speed drive (VSD) would confound the pattern matching algorithm because its power consumption does not have unique steady-state patterns; therefore, different method is required to resolve power consumption of a variable power load from other constant power loads.

VSDs are commonly used in fans and industrial machines for controllability and optimal energy consumption. A typical VSD system is generally comprised of a rectifier, a dc-bus link, an inverter, and an induction motor as shown in Fig. 1. The rectifier front-end usually draws current that is rich in harmonic content and these line current harmonics can be calculated numerically or analytically given system parameters [6]–[9]. An empirically-based VSD mean power estimator has been developed using a correlation function between the real power and the current harmonic powers [4]. However, the correlation function could change about $5-10\%$ from the based case during experiments [3]. One possible source of the deviation is input voltage variation because it affects relative amount of line current harmonics produced by the rectifier [9].

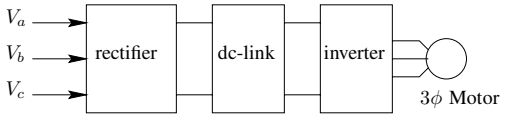

Fig. 1. Typical 3-phase VSD system block diagram

To minimize the estimation error, this paper adapts a switching function method to include the input voltage variation in the estimation. Given system parameters, the switching function method can be used to relate rectified current harmonics to ac-side current harmonics in the harmonic analysis of power converters [10], [11]. Although some system parameters are usually unknown in NILM applications, certain switching functions can be used to create estimating functions for the line-side fundamental current harmonic from other line-side current harmonics.

This paper proposes the switching-function-based power estimator that can resolve power consumption of VSDs among other constant power loads from the aggregate measurement under different input voltage conditions. The paper is organized as followed. First, the NILM system and the empirically-based VSD mean power estimator are briefly explained in section II. Section III introduces a general VSD model. A brief summary of the switching function method is covered in section IV. The switching-function-based estimator is derived in section V. Experimental results are shown in section VI. Finally, the proposed estimator is summarized in section VII.

II. Background

A NILM system monitors multiple loads from a central observation point and extracts information of individual load from current and voltage waveforms. The system block diagram is shown in Fig. 2. Sampled current waveforms are used to compute spectral envelopes or short-time Fourier series coefficients for in-phase and quadrature components of the kth current harmonic denoted by $I_{pk}(t)$ and $I_{qk}(t)$ respectively.

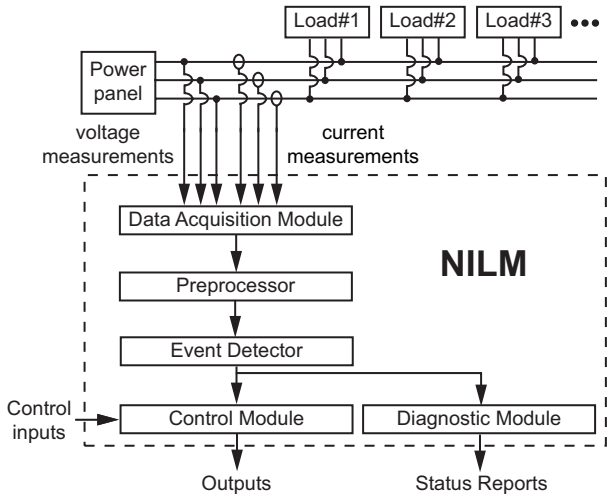

Fig. 2. NILM block diagram

Coefficients $I_{pk}(t)$ and $I_{qk}(t)$ can be computed by

$$I_{pk}(t) = \frac{2}{T} \int_{t-T}^{t} i(\tau) \sin\left(\frac{2\pi k}{T}\tau\right) d\tau, \tag{1}$$

and

$$I_{qk}(t) = -\frac{2}{T} \int_{t-T}^{t} i(\tau) \cos\left(\frac{2\pi k}{T}\tau\right) d\tau, \tag{2}$$

where the variable T is a fundamental time period [1], [5].

The fundamental real and reactive powers can be computed by

$$P_1(t) = \frac{1}{2} V_1 I_{p1}(t) \tag{3}$$

and

$$Q_1(t) = \frac{1}{2} V_1 I_{q1}(t), \tag{4}$$

respectively, where V_1 is the magnitude of the fundamental input voltage. In the case of higher current harmonics, current harmonic power quantities are defined as $P_k(t) = \frac{1}{2} V_1 I_{pk}(t)$ and $Q_k(t) = \frac{1}{2} V_1 I_{qk}(t)$ [4]. These time-varying coefficients are used to detect possible load events by the change of mean method and to match incoming transient and steady-state signals against stored templates in the library [1], [4].

Because of the time-varying nature of the VSD power consumption, the VSD signal content must be removed from the aggregate measurement and the residual signal can be disaggregated using pattern recognition algorithm for constant power loads. Assuming that certain harmonics are uniquely generated by the VSD, these harmonics can be used to estimate the fundamental current harmonic and powers consumed by the VSD from aggregate measurement as proposed in [4].

This paper proposes the switching-function-based VSD power estimator that can adapt estimating functions according to the input voltage as shown in Fig. 3. The proposed estimator

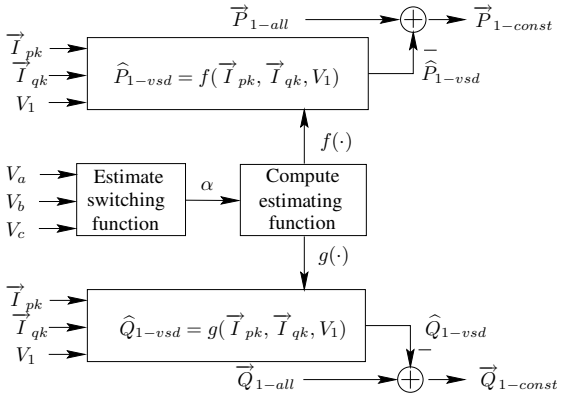

Fig. 3. Switching-function-based VSD power estimator

uses input voltage to approximate a feasible switching function and to create estimating functions for the fundamental current harmonic consumed by the VSD from a finite set of higher harmonics. Finally, the estimator computes the fundamental real and reactive powers consumed by the VSD using (3) and (4) respectively. Algorithm details are shown in next sections.

III. VSD Model

A simple circuit topology that represents a VSD system is shown in Fig. 4 [9]. Three-phase input voltage is converted

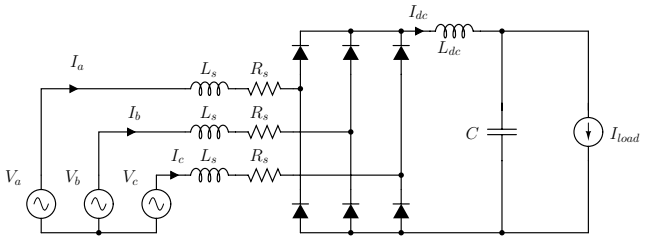

Fig. 4. Typical VSD circuit topology for a voltage-source-inverter type

to dc voltage through an uncontrolled rectifier. A dc-bus capacitor holds the bus voltage for the inverter to generate drive voltage for an induction motor. An optional dc-bus inductor can be installed to filter high frequency harmonics. The inverter is normally operated at a frequency that is much higher than the line frequency. The inverter current seen by the dc-bus capacitor contains both a dc component and high frequency harmonics. However, high frequency current harmonics generated by the inverter are negligible from the ac-side observation [7]. Furthermore, simulation results show that a constant current source I_{load} provides a good representation of an inverter and motor combination for the harmonic analysis in simulations [9].

Typical line current consumed by a VSD exhibits two separate peaks during each half of a line voltage cycle as shown in Fig. 5. In this case, the system is operated in discontinuous current mode (DCM). In frequency domain, the VSD current is mainly consisted of odd harmonics such as fundamental, fifth, seventh, eleventh, and thirteenth harmonics. Assuming these odd harmonics are unique to the VSD; as a

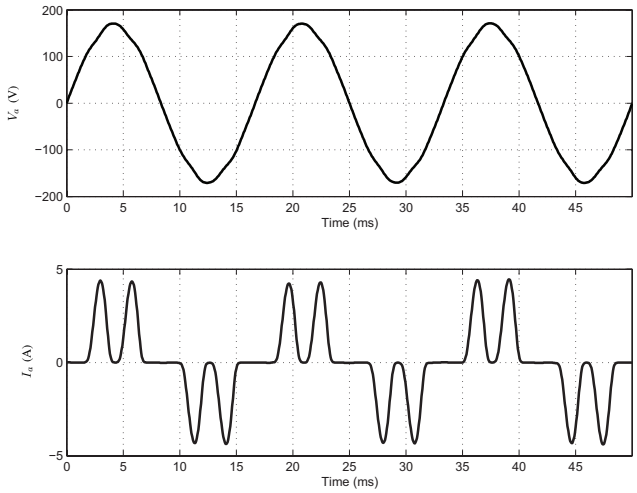

Fig. 5. Typical VSD line current with reference input voltage

result, the estimator can use higher-order odd harmonics to characterize and estimate the fundamental consumed by the VSD from the aggregate measurement.

IV. Switching Function

This section uses the switching function technique to briefly explain the consumption of line current harmonics by the VSD operation. Let phase-A line-to-neutral voltage, $V_{an} = V_1 \sin\theta$, be a reference, where θ is an electrical angle and V_1 is the magnitude of the fundamental voltage. During each voltage cycle, the observed line current on phase-A, I_a, is the result of the modulation of the dc-side current , I_{dc}, by the corresponding switching function, S_a. The switching function represents on/off times of rectifier's switches. Assuming the dc average of the line current is negligible, phase-A line current is given by

$$I_a = S_a I_{dc}. \tag{5}$$

In general, an arbitrary switching function can be represented by Fourier series as

$$S_a = S_0 + \sum_n S_{pn} \sin n\theta - S_{qn} \cos n\theta, \tag{6}$$

where the variable n is the harmonic number, the variable S_0 is the average value, and variables S_{pn} and S_{qn} represent the in-phase and quadrature components of the nth harmonic of the switching function, respectively.

Similarly, the dc-side or rectified current can be represented by another Fourier series as

$$I_{dc} = I_0^{dc} + \sum_m I_{pm}^{dc} \cos m\theta + I_{qm}^{dc} \sin m\theta, \tag{7}$$

where the variable m is the harmonic number, the variable I_0^{dc} is the average current behind the rectifier, and variables I_{pm}^{dc} and I_{qm}^{dc} represent the in-phase and quadrature components of the mth harmonic of the dc-side current, respectively.

The modulation process yields phase-A line current, which can be represented by another Fourier series as

$$I_a = I_0 + \sum_k I_{pk} \sin k\theta - I_{qk} \cos k\theta, \tag{8}$$

where the variable k represents a harmonic number, the variable I_0 is the average line current, and variables I_{pk} and I_{qk} are the in-phase and quadrature components of the line-side kth current harmonic, respectively.

Alternatively, each Fourier series coefficient of the phase current can be written in terms of a weighted sum of the dc-side Fourier series coefficients by substituting (6) and (7) in (5). Mathematically, Fourier series coefficients I_0, I_{pk}, and I_{qk} are given by

$$I_0 = W_{p0} I_p^{dc} + W_{q0} I_q^{dc}, \tag{9}$$

$$I_{pk} = W_{pk}^A I_p^{dc} + W_{qk}^A I_q^{dc}, \tag{10}$$

and

$$I_{qk} = W_{pk}^B I_p^{dc} + W_{qk}^B I_q^{dc}. \tag{11}$$

The column vector I_p^{dc} represents the dc and in-phase components of dc-side harmonics,

$$I_p^{dc} = \begin{bmatrix} I_0^{dc} & I_{p1}^{dc} & I_{p2}^{dc} & I_{p3}^{dc} & \dots \end{bmatrix}^T,$$

and a column vector I_p^{dc} represent quadrature components of dc-side harmonics,

$$I_q^{dc} = \begin{bmatrix} I_{q1}^{dc} & I_{q2}^{dc} & I_{q3}^{dc} & \dots \end{bmatrix}^T.$$

Row vectors $W_{p0}, W_{q0}, W_{pk}^A, W_{qk}^A, W_{pk}^B$, and W_{qk}^B contain weighting coefficients that relate dc-side harmonics to ac-side harmonics. These weighting coefficients can be easily computed from switching function coefficients, S_0, S_{pn}, and S_{qn}. Once both switching function and dc-side harmonics are known, all VSD line-side harmonics can be computed using (9), (10), and (11). Although the exact switching function and dc-side harmonics are not observable in practice, few approximation steps are introduced in the next section to simplify the system, to estimate both switching function and dc-side harmonics, and to derive the proposed VSD power estimator.

V. Estimator derivation

This section fully explains the derivation of the proposed estimator based by dividing the problem into two parts: the estimation of switching function estimation and the estimation of dc-side current harmonics. First, the paper shows how to approximate the switching function in the actual environment and how to select the switching function that can simplify the estimation problem. The estimation of dc-side current harmonics can be done by imposing few constraints on the system. In this paper, the following conditions are assumed:

- the rectifier front-end is operated in discontinuous current mode (DCM),
- a diode behaves like an ideal switch, and
- harmonics used in the estimator are uniquely consumed by the VSD.

A. Switching Function Approximation

There are two main issues in the estimation of the switching function. First, the exact switching function is not observable in practice. Next, the approximate switching function should provide insights and advantages to derive the proposed VSD power estimator.

The actual switching function is defined by switching instants of the diode bridge. In DCM, the switching function can be thought as a window that the input voltage transfers energy to the dc-bus capacitor and the inverter. Therefore, an alternative switching window can be any rectangular window that contains appropriate current pulses for the corresponding line current. For example, under balanced three-phase input voltage without line-side reactance, the diode bridge would switch six times per voltage cycle at $\theta = \frac{\pi}{6} + l\frac{\pi}{3}$, where $l = 0, 1, 2, 3, 4, \text{and}\, 5$. These switching patterns correspond to an ideal switching function that can be used in the estimation theoretically. In general, the input voltage may be unbalanced or distorted because of the line-side reactance. In this case, the ideal switching function may not be the valid choice. The better alternative is the shifted ideal switching function, which is given by

$$S_a = \begin{cases} 1 & \text{for } \alpha \le \theta \le \alpha + \frac{2\pi}{3}, \quad (12a) \\ -1 & \text{for } \alpha + \pi \le \theta \le \alpha + \frac{5\pi}{3}, \quad (12b) \\ 0 & \text{otherwise}, \quad (12c) \end{cases}$$

where the angle α is the minimum angle that allow the shifted ideal switching function to contain all four pulses for phase-A. An example of the approximate switching function is shown in Fig. 6. Fourier series coefficients S_{pn} and S_{qn} of the

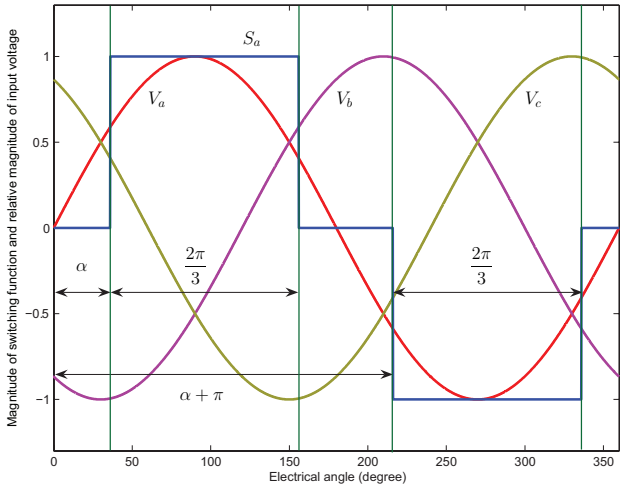

Fig. 6. Approximate switching function

approximate switching function in (12) are given by

$$S_{pn} = -\frac{4}{n\pi}\sin\frac{n\pi}{2}\sin\frac{n\pi}{3}\cos n(\frac{5\pi}{6} + \alpha), \quad (13)$$

and

$$S_{qn} = -\frac{4}{n\pi}\sin\frac{n\pi}{2}\sin\frac{n\pi}{3}\sin n(\frac{5\pi}{6} + \alpha). \quad (14)$$

In this case, weighting coefficients matrices W_{pk}^A, W_{qk}^A, W_{pk}^B, and W_{qk}^B contain lots of zero coefficients. For example, the weighting coefficients matrix for the fundamental current harmonic W_{p1}^A is given by

$$W_{p1}^A = [W_{p1}^A[0], 0, W_{p1}^A[2], 0, W_{p1}^A[4], 0, ...].$$

Furthermore, all line-side triplen harmonics only depend on dc-side even harmonics that are not multiple of six. For example, the weighting vector for the third harmonic W_{p3}^A is given by

$$W_{p3}^A = [\mathbf{0}, 0, W_{p3}^A[2], 0, W_{p3}^A[4], 0, \mathbf{0}, 0, W_{p3}^A[8], ...].$$

Finally, the magnitude of weighting coefficients in matrices W_{pk}^A, W_{qk}^A, W_{pk}^B, and W_{qk}^B are small for $m \ll k$ and $m \gg k$, where m corresponds to the dc-side harmonic number and k represent the ac-side harmonic number. These characteristics of weighting coefficients simplify the system significantly if the shifted ideal switching function can be applied.

B. Harmonic Approximation

This section presents the derivation of the switching-function-based VSD power estimator for the system under different constraints.

1) Balanced Case: In the case of balanced input voltage, the dc-side current contains six identical pulses per one voltage cycle in steady-state. As a result, the dc-side current contains only the dc component and harmonics that are multiple of six. Examples of current and related voltage waveforms in the balanced case are shown in Fig. 7. In this case, harmonic

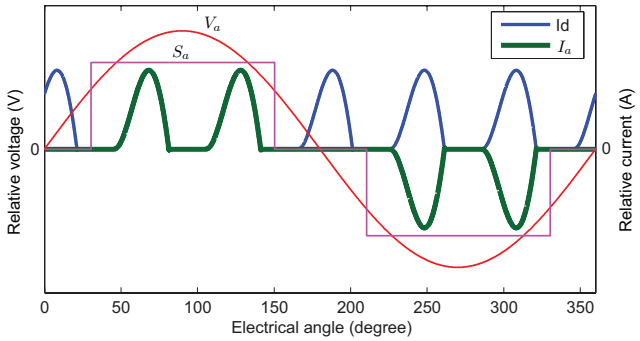

Fig. 7. Examples of current and voltage waveforms in the balanced case.

vectors I_p^{dc} and I_q^{dc} can be reduced to $[I_0^{dc}, I_{p6}^{dc}, I_{p12}^{dc}, ...]^T$ and $[I_{q6}^{dc}, I_{q12}^{dc}, I_{q18}^{dc}, ...]^T$ respectively.

According to the simulation, dc-side high frequency harmonics can be ignored because of two reasons. First, high frequency harmonics are mainly absorbed by the dc-bus filter. In addition, for low-ordered ac-side harmonic, the weighting coefficients for high dc-side harmonics are relatively smaller. Consequently, the harmonic vectors I_p^{dc} and I_q^{dc} can be divided into two parts: main and residual harmonics. Main harmonics include the first M entries of dc-side harmonic vectors represented by $I_p^{dcM} = \overbrace{[I_0^{dc}, I_{p6}^{dc}, I_{p12}^{dc}, ...]}^{\text{M terms}}$ and

$I_q^{dcM} = \overbrace{[I_{q6}^{dc}, I_{q12}^{dc}, I_{q18}^{dc}, ...]}^{\text{M terms}}$. Residual harmonics include all other higher harmonics represented by ΔI_p^{dcM} and ΔI_q^{dcM}. In this case, the ac-side fundamental harmonic components can be approximated as

$$\begin{bmatrix} I_{p1} \\ I_{q1} \end{bmatrix} \approx \begin{bmatrix} W_{p1}^{AM} & W_{q1}^{AM} \\ W_{p1}^{BM} & W_{q1}^{BM} \end{bmatrix} \begin{bmatrix} I_p^{dcM} \\ I_q^{dcM} \end{bmatrix}, \quad (15)$$

where matrices W_{p1}^{AM}, W_{q1}^{AM}, W_{p1}^{BM}, and W_{q1}^{BM} contain weighting coefficients for the fundamental harmonic of the simplified system.

Similarly, ac-side higher current harmonics consumed by the VSD can be expressed as

$$\begin{bmatrix} I_{p-vsd} \\ I_{q-vsd} \end{bmatrix} \approx \begin{bmatrix} W_{p-vsd}^{AM} & W_{q-vsd}^{AM} \\ W_{p-vsd}^{BM} & W_{q-vsd}^{BM} \end{bmatrix} \begin{bmatrix} I_p^{dcM} \\ I_q^{dcM} \end{bmatrix}, \quad (16)$$

where the vector $I_{p-vsd} = \overbrace{[I_{p5}, I_{p7}, I_{p11}, ...]}^{\text{M terms}}$ representing the ac-side, in-phase components uniquely consumed by the VSD, and the vector $I_{q-vsd} = \overbrace{[I_{q5}, I_{q7}, I_{q11}, ...]}^{\text{M terms}}$ representing the ac-side, quadrature components uniquely consumed by the VSD. Matrices W_{p-vsd}^{AM}, W_{q-vsd}^{AM}, W_{p-vsd}^{BM}, and W_{q-vsd}^{BM} contain corresponding weighting coefficients for the VSD higher current harmonics. Let

$$W_1^M = \begin{bmatrix} W_{p1}^{AM} & W_{q1}^{AM} \\ W_{p1}^{BM} & W_{q1}^{BM} \end{bmatrix} \quad (17)$$

and

$$W_{vsd}^M = \begin{bmatrix} W_{p-vsd}^{AM} & W_{q-vsd}^{AM} \\ W_{p-vsd}^{BM} & W_{q-vsd}^{BM} \end{bmatrix}, \quad (18)$$

the estimated fundamental harmonic components consumed by the VSD are given by

$$\begin{bmatrix} \widehat{I}_{p1} \\ \widehat{I}_{q1} \end{bmatrix} = T_1 \begin{bmatrix} I_{p-vsd} \\ I_{q-vsd} \end{bmatrix}, \quad (19)$$

where $T_1 = W_1^M (W_{vsd}^M)^{-1}$.

Because the matrix W_{vsd}^M depends on the shifted angle α, it is possible that the matrix could be come close to singular or poorly conditioned. However, these conditions can be tested off-line and the problem can be mitigated by reducing the dimension of the matrix W_{vsd}^M.

2) General Case: In the actual VSD application, the input voltage may be slightly unbalanced or distorted and the system may never reach steady-state. In this case, all six current pulses may be different and the dc-side current would include all harmonics as shown in Fig. 8. In this case, additional ac-side harmonics are required to accurately estimate dc-side harmonics. Using the approximate switching function, triplen harmonics can be used to estimate additional even dc-side harmonics.

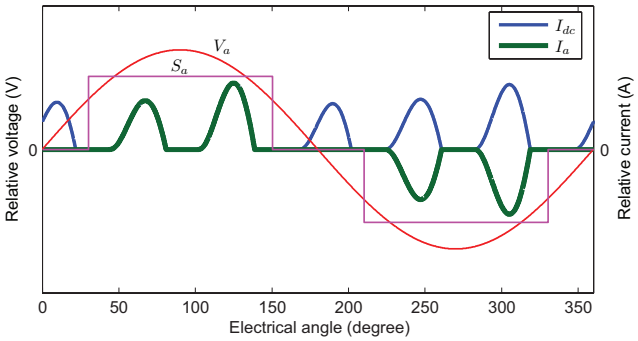

Fig. 8. Examples of current and voltages waveforms and relative magnitude of dc-side harmonics in a general case

Let $I_p^{dcx} = [I_{p2}^{dc}, I_{p4}^{dc}, I_{p8}^{dc}, I_{p10}^{dc}]^T$ be additional dc-side harmonics to be considered and other even harmonics are represented by $\Delta I_p^{dcx} = [I_{p14}^{dc}, I_{p16}^{dc}, I_{p20}^{dc}, ...]^T$. Additional ac-side harmonics used in the estimation are included in the vector $I_{p-x} = [I_{p3}, I_{p9}]^T$. Similar vectors can be written for quadrature components, $I_q^{dcx} = [I_{q2}^{dc}, I_{q4}^{dc}, I_{q8}^{dc}, I_{q10}^{dc}]^T$, $\Delta I_q^{dcx} = [I_{q14}^{dc}, I_{q16}^{dc}, I_{q20}^{dc}, ...]^T$, and $I_{q-x} = [I_{q3}, I_{q9}]^T$. Additional dc-side harmonics change (15) and (16) to

$$\begin{bmatrix} I_{p1} \\ I_{q1} \end{bmatrix} \approx W_1^M \begin{bmatrix} I_p^{dcM} \\ I_q^{dcM} \end{bmatrix} + W_1^x \begin{bmatrix} I_p^{dcx} \\ I_q^{dcx} \end{bmatrix}, \quad (20)$$

and

$$\begin{bmatrix} I_{p-vsd} \\ I_{q-vsd} \end{bmatrix} \approx W_{vsd}^M \begin{bmatrix} I_p^{dcM} \\ I_q^{dcM} \end{bmatrix} + W_{vsd}^x \begin{bmatrix} I_p^{dcx} \\ I_q^{dcx} \end{bmatrix}. \quad (21)$$

Similar equation can be written for triplen harmonics as

$$\begin{bmatrix} I_{p-x} \\ I_{q-x} \end{bmatrix} \approx W_x^x \begin{bmatrix} I_p^{dcx} \\ I_q^{dcx} \end{bmatrix}. \quad (22)$$

Matrices W_1^x, W_{vsd}^x, and W_x^x contain weighting coefficients for the ac-side harmonics. The estimation error in the augmented system using the estimator derived in the balanced case is given by

$$\begin{aligned} \begin{bmatrix} e_{p1} \\ e_{q1} \end{bmatrix} = &(\Delta W_1^M - T_1 \Delta W_{vsd}^M) \begin{bmatrix} \Delta I_p^{dcM} \\ \Delta I_q^{dcM} \end{bmatrix} \\ &+ (W_1^x - T_1 W_{vsd}^x) \begin{bmatrix} I_p^{dcx} \\ I_q^{dcx} \end{bmatrix} \\ &+ (\Delta W_1^x - T_1 \Delta W_{vsd}^x) \begin{bmatrix} \Delta I_p^{dcx} \\ \Delta I_q^{dcx} \end{bmatrix}. \end{aligned} \quad (23)$$

Additional harmonics can be used to minimize the second error term, $(W_1^x - T_1 W_{vsd}^x)[I_p^{dcx}, I_q^{dcx}]^T$. The error correction factor is given as

$$T_{1x} = \left((W_x^x (W_x^x)^T)^{-1} (W_x^x (W_1^x - T_1 W_{vsd}^x)^T) \right)^T. \quad (24)$$

The final estimating function is given by

$$\begin{bmatrix} \widehat{I}_{p1} \\ \widehat{I}_{q1} \end{bmatrix} = T_1 \begin{bmatrix} I_{p-vsd} \\ I_{q-vsd} \end{bmatrix} + T_{1x} \begin{bmatrix} I_{p-x} \\ I_{q-x} \end{bmatrix}. \quad (25)$$

Additional harmonics can be used to increase the accuracy of the estimator without affecting the underlying algorithm. In addition, the algorithm does not require prior knowledge of system parameters and operations. As a result, the estimating functions can be pre-computed and stored in a look-up table to avoid computationally intensive operations such as a matrix inversion routine.

VI. Results and Discussion

This section summarizes experimental results that demonstrate the ability of the switching-function-based VSD power estimator to resolve power consumption of VSD and rectifier loads from other constant power loads. In addition, the estimation results were compared with the empirically-based estimator to compare the improvement.

The experimental setup is consisted of a controllable three-phase voltage source and three electronic loads: a VSD system connected to a dynamometer , a 200-W three-phase rectifier load, and a 50-W light bulb, connected between phase-A and neutral. The experimental setup is shown in Fig. 9.

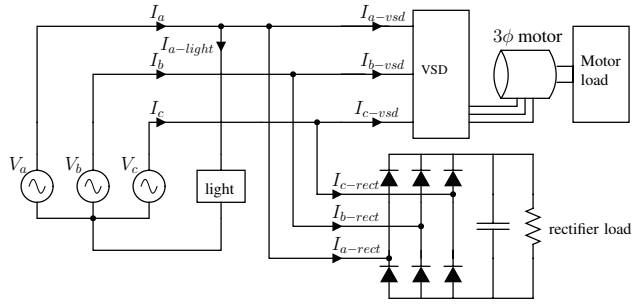

Fig. 9. Experimental setup

For all experiments, the switching-function-based estimator used three in-phase and three quadrature components of ac-side harmonics, specifically, $I_{p-vsd} = [I_{p5}, I_{p7}, I_{p11}]^T$ and $I_{q-vsd} = [I_{q5}, I_{q7}, I_{q11}]^T$. In addition, the third and ninth harmonics were used for the error correction factor, $I_{p-x} = [I_{p3}, I_{p9}]^T$ and $I_{q-x} = [I_{q3}, I_{q9}]^T$.

A. Balanced Input Voltage

First, the switching-function-based VSD power estimator was tested under balanced input voltage case. This input voltage was used to generate the correlation function for the empirically-based estimator. The goal of this test is to demonstrate the ability of the switching-function-based estimator to extract the power consumed by both the VSD and rectifier from the 50-W light bulb during sequence of load operations. Experimental results are shown in Fig. 10. The experimental result in Fig. 10 clearly demonstrates that the switching-function-based estimator can resolve the power

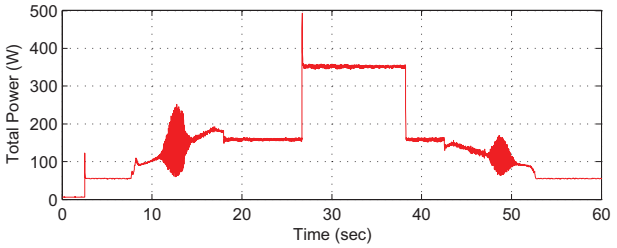

(a) Total power

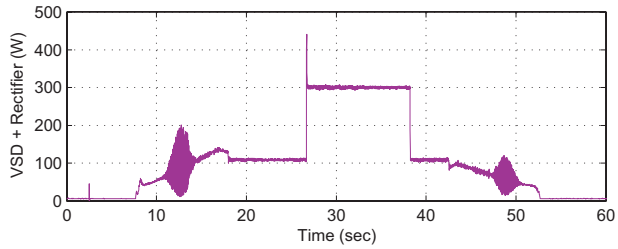

(b) Estimated VSD and rectifier powers

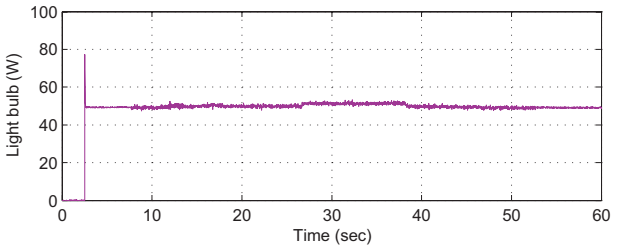

(c) Estimated light bulb power

Fig. 10. Resolving power consumption of VSD and rectifier loads from the 50-W light bulb using the switching-function-based estimator

consumption of VSD and rectifier successfully under balanced input voltage. Small error can be noticed during the light bulb start-up transient because the sharp transient contains higher current harmonics that are used in the VSD estimator. As a result, the assumption that all higher harmonics used in the VSD estimator were exclusively generated by the VSD was violated. More complex method may be applied to minimize the estimation error during transient events of other loads.

On the other hand, the estimated light bulb power using the empirically-based estimator is shown in Fig. 11. The result in

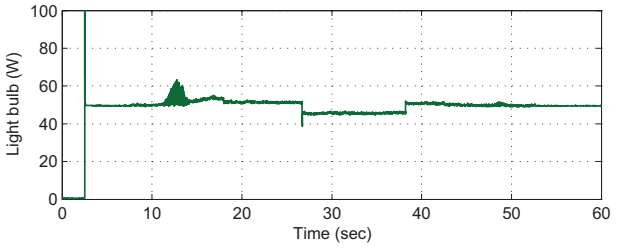

Fig. 11. Estimated light bulb power after the empirically-based estimator has removed powers of the VSD and the rectifier under balanced input voltage

Fig. 11 indicates that the empirically-based estimator produces an error during the rectifier load operation because the rectifier

load had not been characterized.

B. Distorted Input Voltage

To measure the performance of the proposed estimator under input voltage variation, different levels of input voltage distortion were imposed during the experiments to compare performance between the empirically-based and the switching-function-based estimators. In these tests, the VSD was running with constant load and the input voltage was distorted by different amounts of fifth or seventh harmonic in all three phases. The performance is measured by the percentage error of the estimated VSD real power consumption, specifically $\%error = \frac{|P_{vsd} - \widehat{P}_{vsd}|}{P_{vsd}} \times 100$. Experimental results for the fifth and seventh voltage harmonic distortion cases are shown in Fig. 12 and 13 respectively.

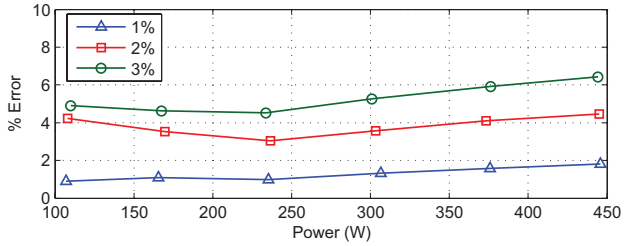

(a) Empirically-based estimator

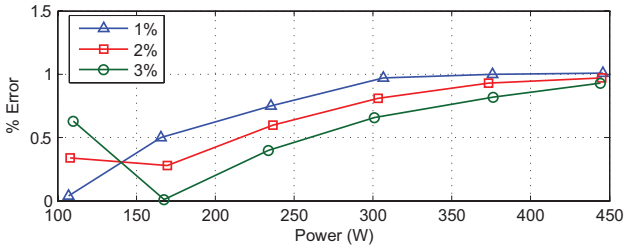

(b) Switching-function-based estimator

Fig. 12. Estimation error comparison between empirically-based estimator and switching-function-based estimator under different levels of fifth voltage harmonic distortion

Experimental results in Fig. 12 and 13 show that the switching-function-based algorithm clearly outperform the empirically-based algorithm across different types of input voltage distortion and load levels.

According to test results, the switching-function-based estimator has demonstrated the ability to resolve power of VSD and rectifier loads from a light bulb load with smaller estimation error. The estimator can adapt to the input voltage distortion and give smaller estimation error than the empirically-based estimator.

VII. Conclusion

This paper has demonstrated that the switching-function-based VSD power estimator shows significant improvement over the empirically-based estimator in resolving the VSD power consumption under small input voltage variation without complete knowledge of system parameters. The proposed

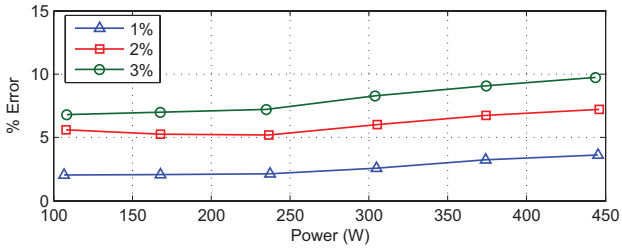

(a) Empirically-based estimator

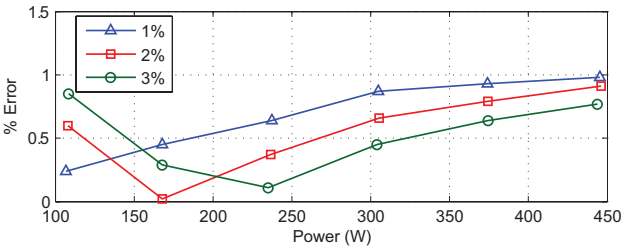

(b) Switching-function-based estimator

Fig. 13. Estimation error comparison between empirically-based estimator and switching-function-based estimator under different levels of seventh voltage harmonic distortion

algorithm enables NILM to work for a larger set of loads. Furthermore, the estimator also shows the ability to track multiple VSDs and rectifier loads together as one rectifier load without additional sensors. This switching function technique could be applied to track other non-linear loads as well.

References

[1] S. B. Leeb, S. R. Shaw, and J. L. Kirtley, "Transient event detection in spectral envelope estimates for nonintrusive load monitoring," *IEEE Trans. Power Del.*, vol. 10, no. 3, pp. 1200–1210, Jul 1995.

[2] A. Cole and A. Albicki, "Nonintrusive identification of electrical loads in a three-phase environment based on harmonic content," in *Proc. IMTC 2000*, vol. 1, May 2000.

[3] K. D. Lee, "Electric load information system based on non-intrusive power monitoring," Ph.d. Thesis, Mass. Inst. of Tech., Jun 2003.

[4] K. D. Lee, S. B. Leeb, L. K. Norford, P. R. Armstrong, J. Holloway, and S. R. Shaw, "Estimation of variable-speed-drive power consumption from harmonic content," *IEEE Trans. Energy Convers.*, vol. 20, no. 3, pp. 566–574, Sep 2005.

[5] S. R. Shaw and C. Laughman, "A kalman-filter spectral envelope preprocessor," submitted for publication in *IEEE. Trans. on Instrum. Meas.* February 2004.

[6] Y. Baghzouz, "An accurate solution to line harmonic distortion produced by ac/dc converters with overlap and dc ripple," *IEEE Trans. Ind. Appl.*, vol. 29, no. 3, pp. 536–540, May/June 1993.

[7] M. Grötzbach and R. Redmann, "Line current harmonics of vsi-fed adjustable-speed drive," *IEEE Trans. Ind. Appl.*, vol. 36, no. 2, pp. 683–690, Mar/Apr 2000.

[8] D. E. Rice, "A detailed analysis of six-pulse converter harmonic currents," *IEEE Trans. Ind. Appl.*, vol. 30, no. 2, pp. 294–304, Mar/Apr 1994.

[9] W. Xu, H. W. Dommel, M. B. Hughes, G. W. Chang, and L. Tan, "Modelling of adjustable speed drives for power system harmonic analysis," *IEEE Trans. Power Del.*, vol. 14, no. 2, pp. 595–601, Apr 1999.

[10] M. Grötzbach and M. Bauta, "Modeling of ac/dc converteres under unbalanced voltage supply using complex switching functions," in *Proc. in Harmonics and Quality of Power*, vol. 2, Nov 2002.

[11] M. Sakui and H. Fujita, "An analytical method for calculating harmonic currents of a three-phase diode-bridge rectifier with dc filter," *IEEE Trans. Power Electron.*, vol. 9, no. 6, pp. 631–637, Nov 1994.